Volume 60
Number 26
4 April 2024
Pages 3459–3596

ChemComm

Chemical Communications

rsc.li/chemcomm

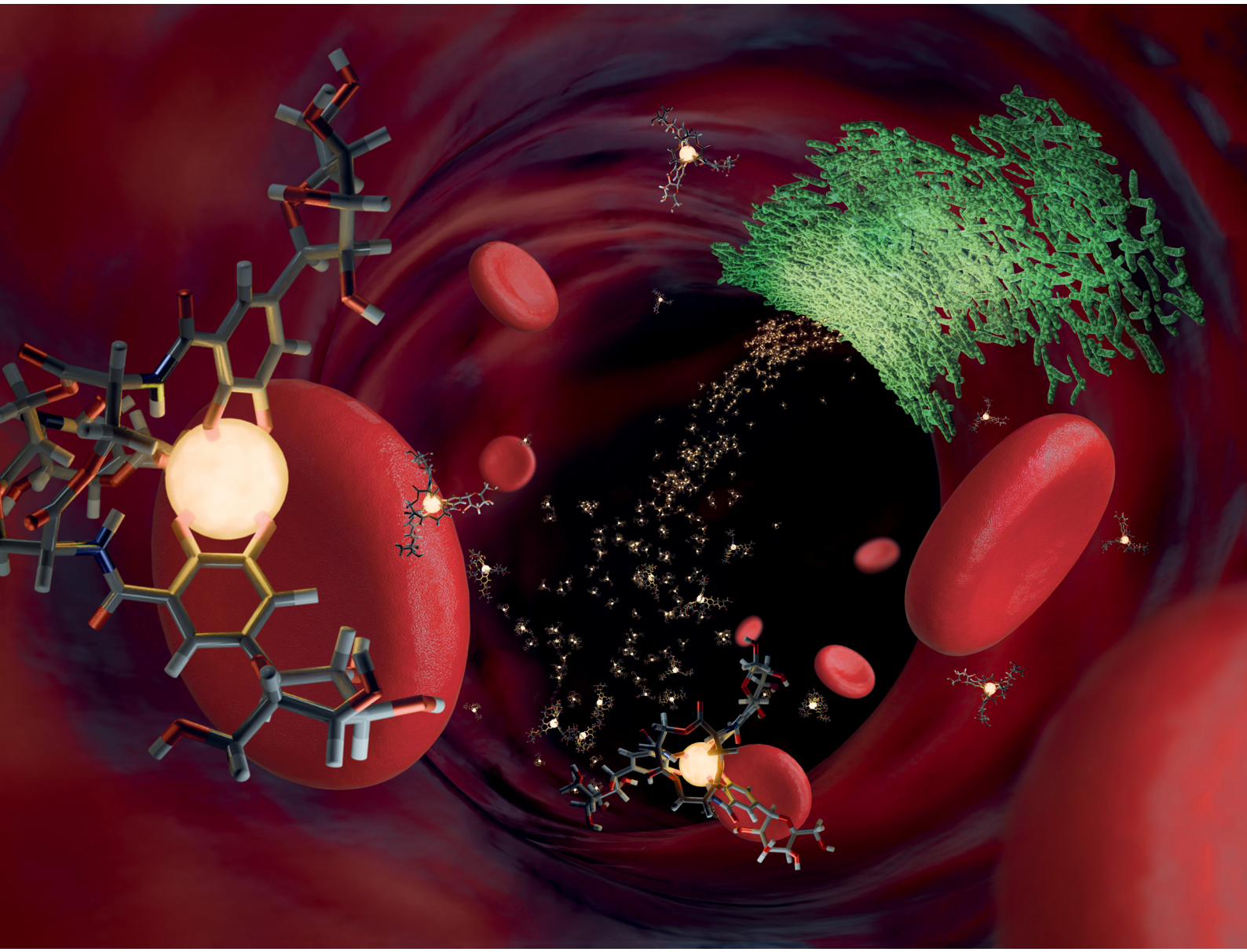

ISSN 1359-7345

ROYAL SOCIETY OF CHEMISTRY

COMMUNICATION

Andreas Faust *et al.*

A novel radiolabelled salmochelin derivative for bacteria-specific PET imaging: synthesis, radiolabelling and evaluation

60 YEARS ANNIVERSARY

ChemComm

COMMUNICATION

View Article Online
View Journal | View Issue

Check for updates

Cite this: *Chem. Commun.*, 2024, **60**, 3507

Received 17th January 2024,
Accepted 14th February 2024

DOI: 10.1039/d4cc00255e

rsc.li/chemcomm

Open Access Article. Published on 15 February 2024. Downloaded on 12/5/2025 8:46:34 PM.
This article is licensed under a Creative Commons Attribution 3.0 Unported Licence.

A novel radiolabelled salmochelin derivative for bacteria-specific PET imaging: synthesis, radiolabelling and evaluation†

Renato Margeta,[a] Sonja Schelhaas,[a] Sven Hermann,[a] Michael Schäfers,[a] Silke Niemann‡[b] and Andreas Faust ‡*[a]

For specific imaging of bacterial infections we aimed at targeting the exclusive bacterial iron transport system *via* siderophore-based radiotracers. *De novo* synthesis and radiolabeling yielded the salmochelin-based PET radiotracer [^{68}Ga]Ga-RMA693, which showed a favourable biodistribution and a bacteria-specific uptake in an animal model of *Escherichia coli* infection.

Bacterial infections such as vascular graft infections, endocarditis, or sepsis remain a leading cause of morbidity and mortality worldwide despite tremendous progress in both diagnosis and treatment. Infections can be difficult to localize and are often associated with nonspecific clinical presentation such as fever and pain. Further, diagnostic blood cultures may be false-negative under or after antibacterial therapy or in the case of bacterial strains that do not grow in blood cultures. These diagnostic challenges have triggered the use of imaging techniques to localize infections. To date, [^{18}F]FDG-positron emission tomography (PET) is available in clinical molecular imaging of infections which relies on the uptake of radiolabelled glucose in activated immune cells given their increased glucose metabolism.[1–3] Thus, this imaging technique does not target bacteria but rather the immune response to bacteria, and thus it is not possible, *e.g.*, to distinguish between sterile inflammation and infection. Besides using bacterial cell wall components like D-amino acids or the bacteria specific uptake of complex carbohydrates PET radiotracers targeting the bacteria-specific iron transport system are a possible way.[4]

An ideal bacteria-specific PET tracer should exclusively be taken up by bacteria and not by host cells. In order to achieve high sensitivity, a molecular signal amplification strategy would be desirable, *e.g.* through transporter-driven cellular uptake and accumulation in the bacterium. In addition, the tracer should be highly stable in blood and serum so that it is not degraded by, *e.g.* enzymes during transport through the blood with only a small amount of the tracer actually reaching the site of infection.[5]

Iron is essential for almost all organisms. To capture enough iron during infections, bacteria have developed specific strategies, such as the production of siderophores, low molecular weight (500–1500 Da) iron chelators with a high affinity for Fe(III). These molecules bind Fe(III) with a higher affinity than eukaryotic transferrin or lactoferrin and can thereby capture Fe(III). Gram-negative bacteria, such as *Escherichia coli* or *Klebsiella pneumoniae*, are surrounded by two membranes, the cytoplasmic cell membrane and the outer membrane. Dedicated bacterial outer membrane transporters have a high affinity for iron-siderophore complexes (*e.g.* FepA for Fe-enterobactin and IroN for Fe-salmochelin) and thereby scavenge these complexes from the environment and transfer them into the periplasmic space. There they are associated to binding proteins and translocated to the cytoplasmic membrane and, *via* specific transporters, to the cytoplasm.[6] Thus, efforts have been made to couple antibiotics to siderophores in order to efficiently deliver them into pathogens *via* the siderophore-mediated iron transport systems in a Trojan horse strategy.[8] For PET a few siderophore-based radiopharmaceuticals have been developed. Desferrioxamine-derivatives labelled with gallium-68 ([^{68}Ga]Ga-DFO-B) showed promising results in *Pseudomonas aeruginosa* and *Staphylococcus aureus* infected mice combined with a fast renal clearance.[9] Several attempts were made to introduce artificial analogues of enterobactin as drug conjugates or imaging tools.[10] In one study a related ^{68}Ga-labelled enterobactin analogue showed limited *in vivo* performance.[11]

Enterobactin as a common siderophore is secreted by *Enterobacteriaceae* such as *E. coli* or *K. pneumoniae*. The host

[a] *European Institute for Molecular Imaging (EIMI), University Münster, Röntgenstraße 16, 48149, Münster, Germany*
[b] *Institute of Medical Microbiology, University Hospital Münster, Domagkstraße 10, 48149, Münster, Germany*

† Electronic supplementary information (ESI) available: Chemical and radiochemical synthesis and all analytical data, *in vivo* stability and biodistribution of the radiotracer, further *in vitro* assays, *etc.* See DOI: https://doi.org/10.1039/d4cc00255e

‡ SN and AF contributed equally and share the senior authorship.

Open Access Article. Published on 15 February 2024. Downloaded on 12/5/2025 8:46:34 PM.
This article is licensed under a Creative Commons Attribution 3.0 Unported Licence.

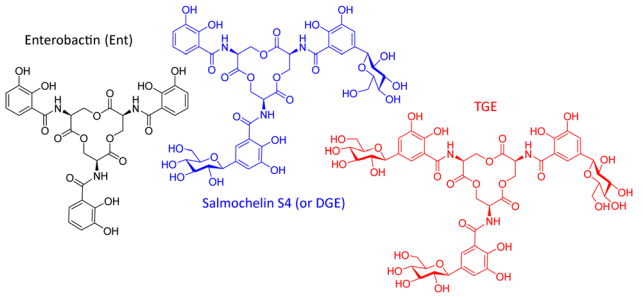

Fig. 1 Structures of selected salmochelin derivatives: enterobactin (Ent), di-(DGE or salmochelin S4), and tri-*C*-glucosylated Ent (**RMA693** or TGE[7]).

counteracts this iron uptake mechanism of the bacteria by producing lipocalin-2. This protein binds to the iron-laden siderophore, preventing its uptake by the bacteria.[12] However, bacteria such as *Salmonella* species, some *Klebsiella* strains and (uro)pathogenic and avian pathogenic *E. coli* strains can produce salmochelin S4, a di-*C*-glucosylated enterobactin (Fig. 1). This so-called stealth siderophore is not bound by lipocalin-2 and thereby allows bacteria to acquire iron even in the presence lipocalin-2.[13]

In a former study salmochelin S4 was used as Trojan horse conjugated with ciprofloxacin.[14] This conjugate as tetradentate ligand showed limited bacterial uptake in comparison to a hexadentate enterobactin-conjugate[15] which underline the importance of the molecular shape for recognition. In our study, we use the gallium-68 (replacing iron) carrying salmochelin-derivative **RMA693** as hexadentate complex to target *E. coli* (Fig. 1). It enables fast and near-quantitative radiolabelling with gallium-68 at room temperature and near-neutral pH.[16] Additionally, the symmetric tri-*C*-glucosylated enterobactin offers a scalable synthesis and complex isolation can be avoided. After radiolabelling with gallium-68 *in vitro* experiments to characterize bacterial uptake and first *in vivo* experiments in mice were performed with successful PET-based imaging of bacterial infections.

Scheme 1 summarizes the total synthesis of **RMA693** as precursor for radiolabelling. Most steps are related to literature-known methods but were optimized to enable large-scale synthesis and purification *via* precipitation or crystallization instead of column chromatography. Starting with the commercially available protected L-serine macrolactonization and subsequent deprotection yielded the trilactone ring **3** in large scale (82%, two steps).[17] To get the iodinated catechol-derivative **6** we selectively mono benzylated[18] the 2,3-dihydroxy benzaldehyde **4** followed by iodination[19] in *para*-position to the phenol for later *C*-glycosylation. Further benzylation, reduction of the benzylaldehyde **7** and silyl protection of the resulting alcohol **8** yielded the key intermediate **9**. Accordingly, we did not perform *C*-glycosylations *via* metal-catalysed cross coupling reactions like Negishi- or Stille-coupling.[20] We lithiated **9** and with glucono-1,5-lactone we built up selectively the β-*C*-glycoside **10** as hemiketal. After reduction of the lactol with triethylsilane in the presence of $BF_3{\cdot}OEt_2$[21] the silylated benzyl alcohol was deprotected and oxidized in a two-step procedure using Dess Martin periodinane and Lindgren-oxidation yielding the carboxylic acid **14**.[22] Again, no column chromatography was necessary, and all steps could be performed on a multigram scale (see ESI† for details). The free amino groups from lactone **3** were combined with carboxylic acid **14** *via* peptide coupling activated by PyAOP and the resulting perbenzylated **RMA693** was deprotected quantitatively under standard conditions yielding the precursor **RMA693** for complexation either with iron or gallium. It was observed that **RMA693** is very sensitive to nucleophiles and oxidizing agents which also others reported during their work on enterobactin.[22] This sensitivity was attributed to the macrolactone ring, which is identical for **RMA693**. Coordination of **RMA693** with tris(2,2,6,6-tetramethyl-3,5-heptanedionato)iron(III) and -gallium(III) yielded nearly quantitatively the corresponding complexes as purple (Fe) and white (Ga) solids (Scheme 2). For manual radiolabelling generator-eluted gallium-68 (350–600 MBq) was neutralized and diluted with PBS-buffer (pH 7.4). After 10 min at 50 °C the precursor was totally consumed and the radiochemical purity of the resulting radiotracer **[^{68}Ga]Ga-RMA693** was higher than 99% (TLC and HPLC). It is stable for at least 120 minutes in the blood serum of mice and humans (Fig. S2, ESI†) and in used media for *in vitro* evaluation (Fig. S4, ESI†).

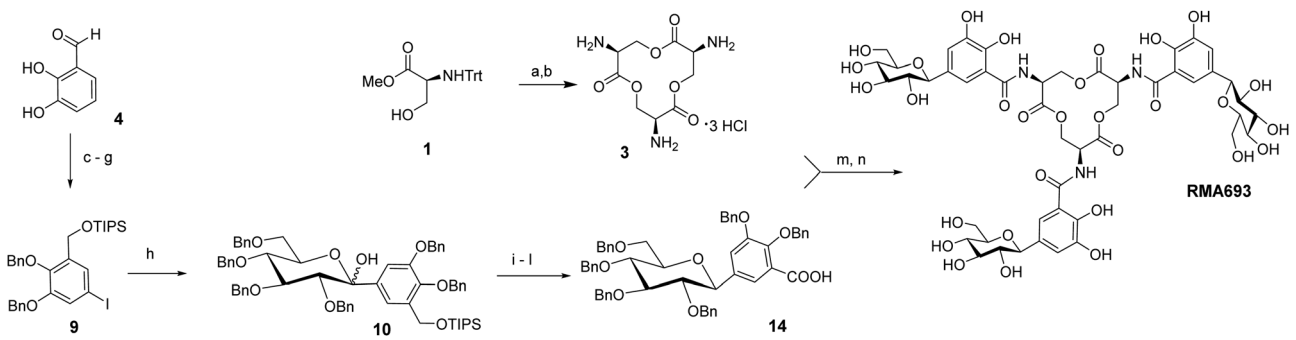

Scheme 1 Synthesis of the precursor **RMA693**: (a) 2,2-dibutyl-[1,3,2]-dioxastannolane, xylene, reflux, 24 h, 84%; (b) 4 M HCl(g)/dioxane, DCM, rt, overnight, 98%, (c) BnBr (1 eq.), NaH, THF, rt, 44%; (d) ICl, $AgNO_3$, Py, $CHCl_3$, 93%; (e) BnBr, K_2CO_3, Me_2CO, reflux, 2 h, 87%; (f) $NaBH_4$, MeOH, 0 °C → rt, 3 h, 96%; (g) TIPSCl, imidazole, DCM, rt, 96%; (h) (1) *n*-BuLi, PhMe, THF, −78 °C; (2) tetra-*O*-Bn-D-glucono-1,5-lactone, −78 °C to rt; (i) Et_3SiH, $BF_3{\cdot}OEt_2$, DCM, −78 °C; (j) conc. $HCl_{(aq)}$, EtOH, 50 °C, 44% (5 steps); (k) DMP, DCM, rt; (l) $NaClO_2$, NH_3SO_3, dioxane, H_2O, rt, 86% (2 steps); (m) PyAOP, DIPEA, ACN, rt, 77%; (n) H_2, $Pd(OH)_2/C$, THF/H_2O 1 : 1, 100%.

 This journal is © The Royal Society of Chemistry 2024

Open Access Article. Published on 15 February 2024. Downloaded on 12/5/2025 8:46:34 PM.
This article is licensed under a Creative Commons Attribution 3.0 Unported Licence.

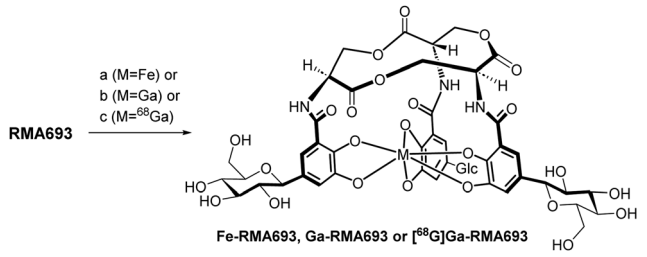

Scheme 2 (a) $Fe(TMHD)_3$, MeOH/EtOAc 1 : 1, rt, 97%; (b) $Ga(TMHD)_3$, MeOH/EtOAc 1 : 1, rt, 95%; (c) $[^{68}Ga][GaCl_4]^-$ (350–600 MBq), PBS-buffer, $NaHCO_{3(aq)}$, 50 °C, 10 min.

In vitro, E. coli ATCC25922 showed uptake of **[^{68}Ga]Ga-RMA693** in contrast to *E. coli* TG1 and also *S. aureus* LS1 (Fig. 2 and Fig. S3, ESI†). While the strain-dependent **[^{68}Ga]Ga-RMA693** accumulation could be detected with as little as 0.1 MBq ml^{-1} (Fig. S3a, ESI†) the uptake of the radiotracer was also shown to be correlated with the amount applied, with 1 MBq ml^{-1} giving a tenfold higher signal (Fig. S3b, ESI†). The tracer was not taken up by *S. aureus* LS1 or by *E. coli* TG1 which demonstrates the bacterial specificity of **[^{68}Ga]Ga-RMA693**, since salmochelin uptake and thus uptake of the newly developed tracer depends on the presence of the specific transporter system. Gram-positive staphylococci such as *S. aureus* as well as *E. coli* TG1, an *E. coli* K-12 derivative, lack such transporters.[23]

When incubated with 0.1 MBq ml^{-1} **[^{68}Ga]Ga-RMA693** in iron-depleted cation-adjusted medium (ID-CAMHB), we observed a 30-fold increase in the accumulation of the tracer in *E. coli* ATCC25922 compared to incubation in iron-containing medium (Fig. S3c, ESI†). Even under these conditions, *E. coli* TG1 showed no uptake of **[^{68}Ga]Ga-RMA693** (Fig. S3c, ESI†). When 1 MBq ml^{-1} tracer was applied, a nearly 10-fold accumulation was achieved, except for *E. coli* TG1. Furthermore, the highest uptake was reached already after one hour of incubation (Fig. 2). In *Enterobacteriaceae*, the uptake of iron by the bacterial cell is strictly regulated and the transport systems are only induced when iron levels are low. As a result, the expression of the salmochelin receptor (IroN) in the outer membrane of the bacteria is increased.[24] This explains the increased and faster uptake of **[^{68}Ga]Ga-RMA693** in iron-depleted medium compared to uptake in iron-containing environment. During infection, the host decreases the accessibility of iron to the bacteria, *e.g.*, by increasing the iron level in macrophages and decreasing it in blood plasma.[25] Due to this nutritional immunity the *in vitro* results imply that the tracer should be sufficiently taken up by bacteria also *in vivo*.

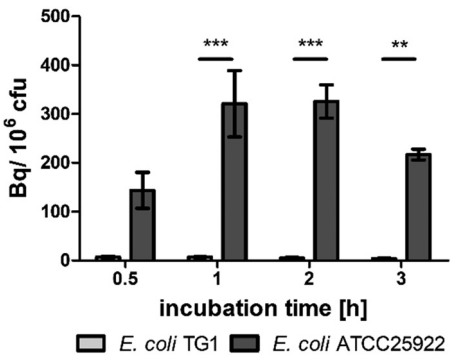

Fig. 2 Strain-dependent *in vitro* uptake of **[^{68}Ga]Ga-RMA693**. *E. coli* TG1 and *E. coli* ATCC25922 were incubated with 1 MBq ml^{-1} **[^{68}Ga]Ga-RMA693** in iron-depleted medium for up to three hours. Tracer uptake was determined using a gamma counter and bacterial colony forming units (cfu) by serial dilution and plating. Data represents the means ± SEM of three (*E. coli* TG1) or four (*E. coli* ATCC25922) independent experiments. *, $p < 0.05$; ***, $p \leq 0.001$; two-way ANOVA followed by Bonferroni post-tests.

To characterize the tracer pharmacokinetics *in vivo*, a biodistribution study in adult CD-1 mice was performed after intravenous injection of ~10 MBq of **[^{68}Ga]Ga-RMA693**. PET imaging demonstrated fast and notable elimination of **[^{68}Ga]Ga-RMA693** from the blood *via* the kidneys into the urinary bladder (Fig. S5a and b, ESI†). Besides this renal route of tracer elimination we did not observe any accumulation of **[^{68}Ga]Ga-RMA693** in other tissues or organs. Quantitative analysis visualized rapid clearance of the tracer from the blood and renal excretion of >90% of the injected dose at the end of the study (90 min post injection, (Fig. S5c, ESI†)). Finally, *in vivo* data were confirmed by *ex vivo* gamma counting of harvested organs and tissues (Fig. S5d, ESI†).

Next, we tested **[^{68}Ga]Ga-RMA693** in a mouse model of bacterial infection. Here, a infection was induced by subcutaneous inoculation of *E. coli* ATCC25922 in the left shoulder region. The *E. coli* TG1 was used as a negative control and was injected in the right shoulder region. 3 h after infection, **[^{68}Ga]Ga-RMA693** was injected intravenously and PET/CT imaging was performed. Images show accumulation of **[^{68}Ga]Ga-RMA693** restricted to the area of *E. coli* ATCC 25922 infection in the left shoulder, in contrast to the *E. coli* TG1 infection on the contralateral side (Fig. 3). Finally, *in vivo* data were confirmed by *ex vivo* gamma counting of harvested tissues (Fig. S6a, ESI†). The bacterial load of the tissue was determined. From both shoulders we recovered living bacteria (in the mouse presented in Fig. 3: left shoulder: 1.51×10^6 colony forming units (cfu) mL^{-1} *E. coli* ATCC25922; right shoulder: 7.2×10^6 *E. coli* TG1 cfu mL^{-1}). To determine whether the **[^{68}Ga]Ga-RMA693** uptake semiquantitatively reflects the number of bacteria at the infection site, we analyzed the correlation between the mean **[^{68}Ga]Ga-RMA693** PET uptake and the number of viable bacteria in the tissue. Indeed, for *E. coli* ATCC 25922 tracer uptake was linearly correlated with the bacterial load ($r = 0.886$, $p < 0.05$). In contrast, there was no such correlation for *E. coli* TG1 ($r = 0.486$, $p = 0.356$) (Fig. S6b and c, ESI†). This result demonstrates that **[^{68}Ga]Ga-RMA693** can be used to selectively detect pathogenic *E. coli*, which are often capable of producing and utilizing salmochelin.

In conclusion, aiming to visualize bacterial infections *in vivo* in a non-invasive and bacteria-specific manner, we have developed a radiotracer for PET imaging targeting the bacterial siderophore-mediated iron transport system. Its scaffold is salmochelin-based, which delivers radioactive gallium instead of iron into the bacterial cell in a Trojan horse strategy. The synthetic development allows large-scale synthesis of tri-glucosylated enterobactin as well as easy and fast ^{68}Ga-radiolabeling with high radiochemical yield and radiochemical purity without further

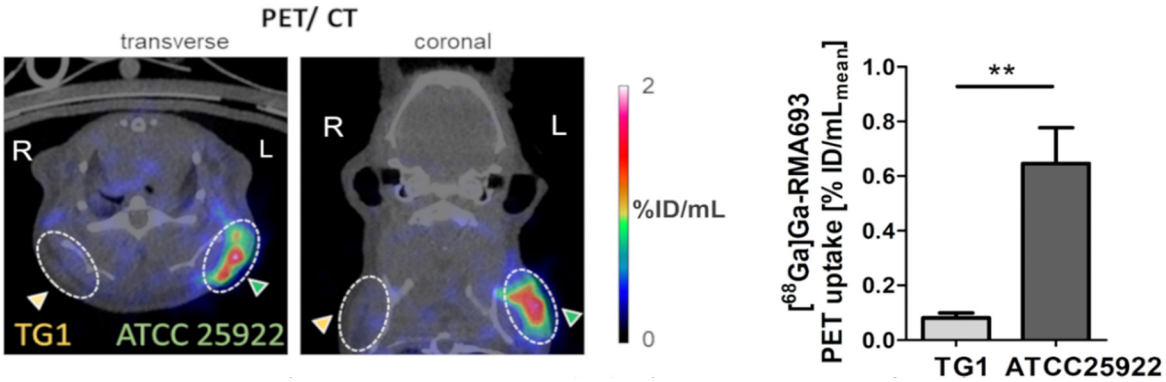

Fig. 3 Strain-dependent *in vivo* uptake of **[^{68}Ga]Ga-RMA693**: (left) representative PET/CT images acquired 90 min after intravenous administration of 10 MBq **[^{68}Ga]Ga-RMA693**. Mice were infected subcutaneously three hours before tracer administration. The arrows indicate the site of infection with two different *E. coli* strains. (right) Quantitative comparison of *in vivo* **[^{68}Ga]Ga-RMA693** uptake between *E. coli* TG1 and *E. coli* ATCC25922. A total of six mice were measured by PET; means ± SEM; **, $p \leq 0.01$; two-tailed Mann–Whitney *U* test. R = right, L = left.

time-consuming purification. We show the strain-dependent uptake of the radiotracer *in vitro* and demonstrate in a first *in vivo* study the potential to specifically detect bacterial infections by PET imaging using our new radiotracer. Further studies are currently ongoing to investigate the sensitivity of the tracer, also in different infectious mouse models.

This work was supported by the Interdisciplinary Centre for Clinical Research (IZKF, University Hospital of Münster, Germany, Fau2-014-17, CoreUnit PIX) and the Collaborative Research Centre (CRC) 1450–431460824, project A04, University of Münster, Germany.

Conflicts of interest

There are no conflicts to declare.

Notes and references

1 E. I. Reinders Folmer, G. C. I. von Meijenfeldt, M. J. van der Laan, A. W. J. M. Glaudemans, R. H. J. A. Slart, B. R. Saleem and C. J. Zeebregts, *Eur. J. Vasc. Endovasc. Surg.*, 2018, **56**, 719.
2 V. Hoerr, M. Franz, M. W. Pletz, M. Diab, S. Niemann, C. Faber, T. Doenst, P. C. Schulze, S. Deinhardt-Emmer and B. Löffler, *Int. J. Med. Microbiol.*, 2018, **308**, 640.
3 E. H. Dibble, D. C. Yoo, G. L. Baird and R. B. Noto, *AJR Am. J. Roentgenol.*, 2019, **213**, 1358.
4 S. Alberto, A. A. Ordonez, C. Arjun, G. K. Aulakh, N. Beziere, E. Dadachova, T. Ebenhan, U. Granados, A. Korde, A. Jalilian, W. Lestari, A. Mukherjee, M. Petrik, T. Sakr, C. L. S. Cuevas, M. M. Welling, J. R. Zeevaart, S. K. Jain and D. M. Wilson, *J. Nucl. Med.*, 2023, **64**, 1676; W. Roll, A. Faust, S. Hermann and M. Schäfers, *J. Nucl. Med.*, 2023, **64**, 59S.
5 A. Axer, S. Hermann, G. Kehr, D. Clases, U. Karst, L. Fischer-Riepe, J. Roth, M. Fobker, M. Schäfers, R. Gilmour and A. Faust, *ChemMedChem*, 2018, **13**, 241.
6 R. C. Hider and X. Kong, *Nat. Prod. Rep.*, 2010, **27**, 637.
7 X. Yu, Y. Dai, T. Yang, M. R. Gagné and H. Gong, *Tetrahedron*, 2011, **67**, 144–151.
8 M. G. P. Page, *Clin. Infect. Diseases*, 2019, **69**, S529.
9 M. Petrik, E. Umlaufova, V. Raclavsky, A. Palyzova, V. Havlicek, J. Pfister, C. Mair, Z. Novy, M. Popper, M. Haiduch and C. Decristoforo, *Eur. J. Nucl. Med. Mol. Imaging*, 2021, **48**, 372.
10 K. Ferreira, H.-Y. Hu, V. Fetz, H. Prochnow, B. Rais, P. P. Müller and M. Brönstrup, *Angew. Chem., Int. Ed.*, 2017, **56**, 8272; P. Klahn, R. Zscherp and C. C. Jimidar, *Synthesis*, 2022, 3499; R. Zscherp, J. Coetzee, J. Vornweg, J. Grundenberg, J. Herrmann, R. Müller and P. Klahn, *Chem. Sci.*, 2021, **12**, 10179.
11 C. Peukert, L. N. B. Langer, S. M. Wegener, A. Tutov, J. P. Bankstahl, B. Karge, F. M. Bengel, T. L. Ross and M. Brönstrup, *J. Med. Chem.*, 2021, **64**, 12359.
12 T. Flo, K. Smith, S. Sato, D. J. Rodriguez, M. A. Holmes, R. K. Strong, S. Akira and A. Aderem, *Nature*, 2004, **432**, 917.
13 B. Bister, D. Bischoff, G. J. Nicholson, M. Valdebenito, K. Schneider, G. Winklemann, K. Hantke and R. D. Süssmuth, *Biometals*, 2004, **17**, 471.
14 M. A. Joaqui-Joaqui, M. K. Pandey, A. Bansal, M. V. Ramakrishnam Raju, F. Armstrong-Pavlik, A. Dundar, H. L. Wong, T. R. DeGrado and V. C. Pierre, *Inorg. Chem.*, 2020, **59**, 12025.
15 T. J. Sanderson, C. M. Black, J. W. Southwell, E. J. Wilde, A. Pandey, R. Herman, G. H. Thomas, E. Boros, A.-K. Duhme-Klair and A. Routledge, *ACS Infect. Dis.*, 2020, **6**, 2532.
16 W. Neumann, M. Sassone-Corsi, M. Raffatellu and E. M. Nolan, *J. Am. Chem. Soc.*, 2018, **140**, 5193.
17 R. J. A. Ramirez, L. Karamanukyan, S. Ortiz and C. G. Gutierrez, *Tetrahedron Lett.*, 1997, **38**, 749–752.
18 I. E. Wrona, A. E. Gabarda, G. Evano and J. S. Panek, *J. Am. Chem. Soc.*, 2005, **127**, 15026–15027.
19 A. V. Joshua, S. K. Sharma and D. N. Abrams, *Synth. Commun.*, 2008, **38**, 434–440.
20 H. Gong and M. R. Gagné, *J. Am. Chem. Soc.*, 2008, **130**, 12177–12183; F. Zhu, J. Rodriguez, T. Yang, I. Kevlishvili, E. Miller, D. Yi, S. O'Neill, M. J. Rourke, P. Liu and M. A. Walczak, *J. Am. Chem. Soc.*, 2017, **139**, 17908–17922; E. J. Wilde, E. V. Blagova, T. S. Sanderson, D. J. Raines, R. P. Thomas, A. Routledge, A. K. Duhme-Klair and K. S. Wilson, *J. Inorg. Biochem.*, 2019, **190**, 75–84.
21 T. C. Ho, H. Kamimura, K. Ohmori and K. Suzuki, *Org. Lett.*, 2016, **18**, 4488–4490.
22 T. Zheng, J. L. Bullock and E. M. Nolan, *J. Am. Chem. Soc.*, 2012, **134**, 18388–18400.
23 M. Valdebenito, A. L. Crumbliss, G. Winkelmann and K. Hantke, *Int. J. Med. Microbiol.*, 2006, **296**, 513–520; K. Hantke, G. Nicholson, W. Rabsch and G. Winkelmann, *Proc. Natl. Acad. Sci.*, 2003, **100**, 3677–3682; J. E. Cassat and E. P. Skaar, *Semin. Immunopathol.*, 2012, **34**, 215–235.
24 A. R. Mey, C. Gómez-Garzón and S. M. Payne, *EcoSal Plus*, 2021, **9**, eESP00342020.
25 R. Golonka, B. S. Yeoh and M. Vijay-Kumar, *J. Innate Immun.*, 2019, **11**, 249–262.

Open Access Article. Published on 15 February 2024. Downloaded on 12/5/2025 8:46:34 PM.
This article is licensed under a Creative Commons Attribution 3.0 Unported Licence.

 This journal is © The Royal Society of Chemistry 2024